

## DO LY $\alpha$ ABSORBERS CO-ROTATE WITH GALAXY DISKS?

DAVID M. FRENCH, BART P. WAKKER

Department of Astronomy, University of Wisconsin, Madison, WI 53706, USA

### ABSTRACT

We present results of a study comparing the relative velocity of Ly $\alpha$  absorbers to the rotation direction and velocity of nearby galaxy disks. We find...

*Keywords:* galaxies:intergalactic medium, galaxies:evolution, galaxies:halos, quasars: absorption lines

### 1. INTRODUCTION

Our current  $\Lambda$ CDM cosmology picture describes galaxies forming hierarchically out of overdensities in the underlying dark matter distribution. As matter is funneled toward a growing galaxy, conservation of angular momentum redistributes the angular momentum in this gas to match that of the halo and underlying dark matter as the gas is shock-heated and slowly cools. As this infalling gas is responsible for birthing and continuing to feed the galaxies, it is expected that the extended gaseous halos should rotate in the same sense as both the galactic disks and dark matter halos. Galaxy rotation curves have been observed to extend at constant velocity out to... (cite...). It becomes increasingly difficult to measure gas rotation much farther from this however as the density rapidly decreases. Within this region the galaxy disks transition into circumgalactic medium (CGM), and eventually the CGM merges with the intergalactic medium (IGM). At what point, however, does the surrounding medium cease to circulate with the galaxy?

HYDRO? simulations such as those by [Stewart et al. \(2011, 2013\)](#) suggests that the bulk CGM kinematics out to (WHAT DISTANCE) may circulate, and that absorption in intervening QSO sightlines should be able to accurately capture this rotation signature. Observational confirmation, however, has been inconclusive. Côté et al. 2005 probed the halos of nine galaxies using *HST* observed background QSOs, finding large warps would be needed to explain the velocity of *H i* absorbers by an extended rotating disk. [Wakker & Savage \(2009\)](#) compiled a sample of 4 galaxy-QSO systems from the literature, finding only 1/4 of Ly $\alpha$  absorbers appeared to co-rotate with the associated galaxy disk. Approaching the question from a different angle, [Bowen et al. \(2016\)](#) probed the halo of a single galaxy, NGC1097, with 4 nearby QSO sightlines, and suggests that an extended, slowly rotating disk with additional inflowing IGM material best matches observations.

Numerous studies have shown a correlation between equivalent width and decreasing velocity difference between galaxies and IGM absorbers (e.g., [French &](#)

[Wakker 2017](#), MORE).

To make progress here, we have obtained rotation curves for 12 nearby spiral galaxies which are located within 500 kpc of a background QSO observed by the Cosmic Origins Spectrograph (COS) on *HST*.

We have augmented this new sample with additional galaxies with known rotation velocity and orientation from the literature. In Section 2 we describe the selection and reduction of both SALT and COS spectra. We then discuss each galaxy-QSO system in detail in Section 3, and introduce our halo-velocity model for interpreting these systems in Section 4. In Section 5 we discuss the overall results of this exercise and present a physically-motivated interpretation of these results. See Section 6 for a summary of our results and conclusions.

### 2. DATA AND ANALYSIS

#### 2.1. SALT Data

Our sample contains 12 galaxies observed with the Southern African Large Telescope (SALT) Robert Stobie Spectrograph (RSS) in longslit mode. These 12 were selected from a larger pool of 48 submitted targets by the SALT observing queue. These 48 possible targets were chosen for their proximity to background QSOs whose spectra contained promising Ly $\alpha$  lines. Finally, we only included galaxies with  $z \leq 0.33$  ( $cz \leq 10,000$  km s<sup>-1</sup>), angular sizes less than 6' to enable easy sky subtraction without taking additional exposures, and surface brightnesses sufficient to keep exposure times below  $\sim 1300$ s. Table 2 summarizes these observations. Data was taken for 2 additional galaxies, NGC3640 and NGC2962, but proved unusable due to issues with spectral identification and low signal-to-noise (respectively).

All SALT galaxy spectra were reduced and extracted using the standard PySALT reduction package (CITATION), which includes procedures to prepare the data, correct for gain, cross-talk, bias, and overscan, and finally mosaic the images from the 3 CCDs. Next, we rectify the images with wavelength solutions found via Ne and Ar arc lamp spectra line identification. Finally, we perform a basic sky subtraction using an off-sky portion of the spectrum, and extract 5-10 pixel wide

Target	Galaxy	R.A.	Dec.	$z$	Program	Grating	Obs ID	Obs Date	$T_{exp}^*$ [ks]	S/N* [1238]
(1)	(2)	(3)	(4)	(5)	(6)	(7)	(8)	(9)	(10)	(11)
1H0419-577	NGC1566	04 26 00.7	-57 12 02.0	0.10400	11686	G130M	Obs ID	Obs Date	20429	75
1H0419-577	NGC1566	04 26 00.7	-57 12 02.0	0.10400	11686	G160M	Obs ID	Obs Date	15934	55
HE0429-5343	NGC1566	04 30 40.0	-53 36 56.0	0.04001	12275	G130M	Obs ID	Obs Date	2067	12
HE0435-5304	NGC1566	04 36 50.9	-52 58 47.0	0.42616	11520	G130M	Obs ID	Obs Date	8372	12
HE0435-5304	NGC1566	04 36 50.9	-52 58 47.0	0.42616	11520	G160M	Obs ID	Obs Date	8935	9
RBS567	NGC1566	04 39 38.7	-53 11 31.0	0.24300	11520	G130M	Obs ID	Obs Date	8176	17
RBS567	NGC1566	04 39 38.7	-53 11 31.0	0.24300	11520	G160M	Obs ID	Obs Date	8933	11
HE0439-5254	NGC1566	04 40 12.0	-52 48 18.0	1.05300	11520	G130M	Obs ID	Obs Date	8402	18
HE0439-5254	NGC1566	04 40 12.0	-52 48 18.0	1.05300	11520	G160M	Obs ID	Obs Date	8935	13
H1101-232	NGC3513	11 03 37.7	-23 29 31.0	0.18600	12025	G130M	Obs ID	Obs Date	13341	16
H1101-232	NGC3513	11 03 37.7	-23 29 31.0	0.18600	12025	G160M	Obs ID	Obs Date	13296	10
SDSSJ112005.00+041323.0	NGC3633	11 20 05.0	+04 13 23.0	0.54689	12603	G130M	Obs ID	Obs Date	4708	9
RX_J1121.2+0326	CGCG039-137	11 21 14.0	+03 25 47.0	0.15200	12248	G130M	Obs ID	Obs Date	2695	5
RX_J1121.2+0326	NGC3633	11 21 14.0	+03 25 47.0	0.15200	12248	G130M	Obs ID	Obs Date	2695	5
RX_J1121.2+0326	CGCG039-137	11 21 14.0	+03 25 47.0	0.15200	12248	G160M	Obs ID	Obs Date	4741	4
RX_J1121.2+0326	NGC3633	11 21 14.0	+03 25 47.0	0.15200	12248	G160M	Obs ID	Obs Date	4741	4
SDSSJ112224.10+031802.0	CGCG039-137	11 22 24.1	+03 18 02.0	0.47528	12603	G130M	Obs ID	Obs Date	7588	10
3C273.0	NGC4536	12 29 06.7	+02 03 09.0	0.15834	12038	G130M	Obs ID	Obs Date	4002	111
3C273.0	NGC4536	12 29 06.7	+02 03 09.0	0.15834	1140	G160M	Obs ID	Obs Date	30028	55
HE1228+0131	NGC4536	12 30 50.0	+01 15 23.0	0.11700	11686	G130M	Obs ID	Obs Date	11036	61
HE1228+0131	NGC4536	12 30 50.0	+01 15 23.0	0.11700	11686	G160M	Obs ID	Obs Date	11029	45
LBQS1230-0015	NGC4536	12 33 04.1	-00 31 34.0	0.47095	11598	G130M	Obs ID	Obs Date	10323	13
LBQS1230-0015	NGC4536	12 33 04.1	-00 31 34.0	0.47095	11598	G160M	Obs ID	Obs Date	5896	7
PG1302-102	NGC4939	13 05 33.0	-10 33 19.0	0.27840	12038	G130M	Obs ID	Obs Date	5979	27
PG1302-102	NGC4939	13 05 33.0	-10 33 19.0	0.27840	12038	G160M	Obs ID	Obs Date	6867	34
SDSSJ135726.27+043541.4	NGC5364	13 57 26.3	+04 35 41.0	1.23453	12264	G130M	Obs ID	Obs Date	14148	15
SDSSJ135726.27+043541.4	NGC5364	13 57 26.3	+04 35 41.0	1.23453	12264	G160M	Obs ID	Obs Date	28206	12
QSO1500-4140	NGC5786	15 03 34.0	-41 52 23.0	0.33500	11659	G130M	Obs ID	Obs Date	9258	9
SDSSJ151237.15+012846.0	UGC09760	15 12 37.2	+01 28 46.0	0.26625	12603	G130M	Obs ID	Obs Date	7590	6
RBS1768	ESO343-G014	21 38 49.9	-38 28 40.0	0.18299	12936	G130M	Obs ID	Obs Date	6962	24
RBS1768	ESO343-G014	21 38 49.9	-38 28 40.0	0.18299	12936	G160M	Obs ID	Obs Date	3837	11
MRC2251-178	MCG-03-58-009	22 54 05.9	-17 34 55.0	0.06609	12029	G130M	Obs ID	Obs Date	5515	42
MRC2251-178	MCG-03-58-009	22 54 05.9	-17 34 55.0	0.06609	12029	G160M	Obs ID	Obs Date	7125	30
RBS2000	IC5325	23 24 44.7	-40 40 49.0	0.17359	13448	G130M	Obs ID	Obs Date	5046	18
RBS2000	IC5325	23 24 44.7	-40 40 49.0	0.17359	13448	G160M	Obs ID	Obs Date	5726	12
RX_J1017.5+4702	NGC3198	10 17 31.0	+47 02 25.0	0.33544	13314	G130M	Obs ID	Obs Date	8655	12

**Table 1.** COS targets in this sample. \*Total exposure time and S/N ratio is given for multi-orbit exposures.

1-D strips from the reduced 2-D spectrum.

For each 1-D spectrum, we identify the H $\alpha$  emission lines and perform a non-linear least-squares Voigt profile fit using the Python package LMFIT<sup>1</sup>. The line centroid and  $1\sigma$  standard errors are returned, and these fits are then shifted to rest-velocity based on the galaxy systemic redshift and heliocentric velocity corrections are calculated with the IRAF rvcorrect procedure. The final rotation velocity is calculated by then applying the

inclination correction,  $v_{rot} = v/\sin(i)$ . Final errors are calculated as a quadrature sum of  $1\sigma$  fit errors, systemic redshift error, and inclination uncertainty as follows:

$$\sigma^2 = \left(\frac{\partial v_{rot}}{\partial \lambda_{obs}}\right)^2 (\Delta \lambda_{obs})^2 + \left(\frac{\partial v_{rot}}{\partial v_{sys}}\right)^2 (\Delta v_{sys})^2 + \left(\frac{\partial v_{rot}}{\partial i}\right)^2 (\Delta i)^2, \quad (1)$$

where  $\Delta \lambda_{obs}$ ,  $\Delta v_{sys}$ , and  $\Delta i$  are the errors in observed

<sup>1</sup> <http://cars9.uchicago.edu/software/python/lmfit/contents.html>

line center, galaxy redshift, and inclination, respectively.

We determine the inclination error by calculating the standard deviation of the set of all axis ratio values available in NED for each galaxy. The final physical scale is calculated using the SALT image scale of 0.1267 arcsec/pixel, multiplied by the 4-pixel spatial binning, and converted to physical units using a redshift-independent distance if available, and a Hubble flow estimate if not. We adopt a Hubble constant of  $H_0 = 71 \text{ km s}^{-1} \text{ Mpc}^{-1}$  throughout.

Finally, we calculate our approaching and receding velocities via a weighted mean of the outer 1/2 of each rotation curve, with errors calculated as weighted standard errors in the mean. Our final redshifts are calculated by forcing symmetric rotation, such that the outer 1/2 average velocity for each side matches in magnitude. See Figure ?? for an example.

## 2.2. COS Spectra

The Barbara A. Mikulski Archive for Space Telescopes (MAST) archives yield 19 QSO targets observed by COS which lie within 500 kpc of our SALT galaxies. These targets vary widely in signal-to-noise from approximately 5 to 100 due to our choosing them based only on their proximity to galaxies with known rotation. The reduction procedure for these spectra follow those described by French & Wakker (2017) and Wakker et al. (2015). In short, spectra are processed with CALCOS vXXXX? and combined via the method of Wakker et al. (2015), which helps corrects the COS wavelength scale misalignments produced by CALCOS. Multiple exposures are combined via alignment with Galactic 21cm absorption spectra and summing total counts per pixel before converting to flux. The COS instrument is described in detail by Green et al. (2012).

## 3. HALO ROTATION MODEL

In order to better understand how QSO sightlines probe intervening velocity structure we have developed a simple halo gas rotation model. This model is seeded by an observed rotation curve (or whatever rotation curve-esque data suits ones fancy). This input curve is then interpolated and extended out to  $2R_{vir}$  based on the average velocity of the outer 1/2 radius. Next, we project this interpolated rotation curve onto a plane oriented to a faux QSO sightline identically to the input galaxy-QSO pair orientation. By stacking multiple rotation-planes in the galaxy z-axis direction, we then create a simple cylindrical rotating halo model. Finally, each rotation-plane in the stack is projected onto the faux sightline. The result is a function representing the rotation velocity encountered by the sightline as a function of velocity (or distance) along it.

For each galaxy-QSO pair we created 2 rotation models: 1) a purely cylindrical halo extending  $2R_{vir}$  in height and  $3R_{vir}$  in radius, and 2) a cylindrical model extending  $2R_{vir}$  in height and  $3R_{vir}$  in radius with rotation velocities which smoothly decline based on a NFW profile fit (Navarro et al. 1996, 1997).

## 4. SALT GALAXIES

### 4.1. CGCG039-137

CGCG039-137 is an isolated Scd type galaxy with a measured systemic velocity of  $6918 \pm 24 \text{ km s}^{-1}$  and inclination of  $63^\circ$ . There are two associated sightlines: RX\_J1121.2+0326 at an impact parameter of 99 kpc and azimuth angle of  $71^\circ$  on the receding side, and SDSSJ112224.10+031802.0 at 491 kpc and  $24^\circ$  on the approaching side. Ly $\alpha$  absorption is detected in both sightlines within  $400 \text{ km s}^{-1}$  of CGCG039-137.

Towards RX\_J1121.2+0326 we detect Ly $\alpha$  at  $6975 \text{ km s}^{-1}$ , which, at  $\Delta v = 57 \text{ km s}^{-1}$ , lies well within the range of projected velocities consistent with co-rotation. The absorber detected toward SDSSJ112224.10+031802.0 occurs at a more distant  $6606 \text{ km s}^{-1}$  ( $\Delta v = -312 \text{ km s}^{-1}$ ). Although this absorber has the correct sign for co-rotation (blue-ward on the approaching side of the disk), the large velocity difference and impact parameter make it unlikely that this absorption can be linked to coherent halo rotation.

### 4.2. ESO343-G014

ESO343-G014 is an edge on spiral galaxy with a measured systemic velocity of  $9138.9 \pm 31.7 \text{ km s}^{-1}$ . It has a smaller neighboring galaxy, 2MASXJ21372816-3824412, located north of it's major axis at a projected distance of 216 kpc and velocity of 9129. The nearest sightline is towards RBS1768 at an impact parameter of 466kpc and  $74^\circ$  azimuth angle on the approaching side. We detect 3 Ly $\alpha$  absorption lines within  $300 \text{ km s}^{-1}$  of ESO343-G014 (at 9308, 9360, and  $9434 \text{ km s}^{-1}$ ). All of these are anti-aligned with the rotation of ESO343-G014, but unfortunately the presence of 2MASXJ21372816-3824412 makes it difficult to attribute this gas solely to ESO343-G014. Additionally, this gas could be attributed to either the approaching or receding side of the disk due to the large impact parameter and high azimuth angle of the sightline.

### 4.3. IC5325

IC5325 is a face-on SAB(rs)bc type galaxy with a measured velocity of  $1511.9 \pm 8.4 \text{ km s}^{-1}$ . It's inclination is just high enough ( $25^\circ$ ) to obtain a reasonable rotation curve. The closest neighboring galaxy is ESO347-G020 to the Southeast at 306 kpc and a heliocentric velocity of  $1745 \text{ km s}^{-1}$ . Three other much smaller galaxies are also located  $\sim 450 \text{ kpc}$  to the Southwest. We detect Ly $\alpha$  absorption at  $1598 \text{ km s}^{-1}$ ,  $\Delta v = 86 \text{ km s}^{-1}$  in the spectrum towards RBS2000 at an impact parameter of 314 kpc and azimuth angle of  $64^\circ$  on the approaching side. While this velocity is anti-aligned with the rotation the disk gas, the low inclination angle of IC5325 leads to a highly uncertain position angle. Without additional observations, we cannot say for certain if the location of RBS2000 actually lies on the approaching or receding side. This position angle uncertainty also means our SALT rotation curve is a lower limit on the true rotation velocity of IC5325.

Galaxy	R.A.	Dec.	$cz$ ( $\text{km s}^{-1}$ )	Type	Grating	$V_{\text{rot}}$ [ $\text{km s}^{-1}$ ]	$V_{\text{rot}}/\sin(i)$ [ $\text{km s}^{-1}$ ]	Obs Date	$T_{\text{exp}}$ [ks]
(1)	(2)	(3)	(4)	(5)	(6)	(7)	(8)	(9)	(10)
CGCG039-137	11 21 26.95	+03 26 41.68	$6918 \pm 24$	Scd	PG2300	$132 \pm 16$	$139 \pm 26$	05 11 2016	700
ESO343-G014	21 37 45.18	-38 29 33.22	$9139 \pm 32$	S	PG2300	$203 \pm 32$	$203 \pm 32$	05 16 2016	1000
IC5325	23 28 43.43	-41 20 0.49	$1512 \pm 8$	SAB(rs)bc	PG2300	$53 \pm 5$	$125 \pm 39$	05 17 2016	600
MCG-03-58-009	22 53 40.85	-17 28 44.00	$9015 \pm 19$	Sc	PG2300	$150 \pm 12$	$171 \pm 23$	05 16 2016	1200
NGC1566	04 20 0.42	-54 56 16.12	$1502 \pm 15$	SAB(rs)bc	PG2300	$64 \pm 8$	$195 \pm 47$	10 18 2016	400
NGC3513	11 03 46.08	-23 14 43.8	$1204 \pm 12$	SB(s)c	PG2300	$11 \pm 10$	$22 \pm 24$	05 26 2016	600
NGC3633	11 20 26.22	+03 35 8.20	$2587 \pm 7$	SAa	PG2300	$149 \pm 6$	$157 \pm 9$	05 11 2016	1200
NGC4536	12 34 27.05	+02 11 17.30	$1867 \pm 33$	SAB(rc)bc	PG2300	$129 \pm 9$	$148 \pm 41$	05 11 2016	1300
NGC4939	13 04 14.39	-10 20 22.60	$3093 \pm 33$	SA(s)bc	PG2300	$204 \pm 25$	$275 \pm 66$	05 14 2016	500
NGC5364	13 56 12.00	+05 00 52.09	$1238 \pm 17$	SA(rs)bc pec	PG2300	$130 \pm 13$	$155 \pm 22$	05 11 2016	700
NGC5786	14 58 56.26	-42 00 48.10	$2975 \pm 22$	SAB(s)bc	PG2300	$156 \pm 10$	$172 \pm 25$	05 11 2016	250
UGC09760	15 12 02.44	+01 41 55.46	$2094 \pm 16$	Sd	PG2300	$46 \pm 10$	$46 \pm 16$	05 11 2016	500

**Table 2.** SALT targeted galaxies. Columns are as follows: 1) the galaxy name, 2), 3) R.A., Dec. in J2000, 4) galaxy systemic velocity, 5) morphological type (RC3), 6) RSS grating used, 7) approaching side velocity, 8) receding side velocity, 9) observation date, 10) exposure time, and 11) S/N of the H $\alpha$  or Ca H&K lines.

#### 4.4. MCG-03-58-009

MCG-03-58-009 is a massive and very isolated Sc type galaxy at a measured velocity of  $9015 \pm 19 \text{ km s}^{-1}$  and inclination angle of  $49^\circ$ . A weak Ly $\alpha$  absorber is detected at  $9029 \text{ km s}^{-1}$  towards MRC2251-178, which lies 355 kpc away at an azimuth angle of  $71^\circ$  on the receding side. Although this absorber matches the velocity direction expected for co-rotation, the velocity difference ( $\Delta v = 14 \text{ km s}^{-1}$ ) is within the systemic velocity uncertainty. The relative weakness of this absorber ( $\text{EW} = 62 \pm 4 \text{ m\AA}$ ) is somewhat surprising given it's proximity (just outside of  $1 R_{\text{vir}}$ ) to a massive galaxy. If this is representative of an isolated system such as MCG-03-58-009, then we should expect the halo rotational velocity to approach systemic by  $1 R_{\text{vir}}$ .

#### 4.5. NGC1566

NGC1566 is well sampled (5 nearby QSO sightlines), but unfortunately also part of a complex environment of neighboring galaxies. We detect Ly $\alpha$  in all 5 of these sightlines. The farthest three, HE0439-5254, RBS567, and HE0435-5304, are clustered close together to the northeast of NGC1566 at  $\gtrsim 395 \text{ kpc}$  and azimuth angles of  $\sim 60^\circ$ .

HE0429-5343 is in the same direction and azimuth angle but closer at  $\rho = 256 \text{ kpc}$ , and shows Ly $\alpha$  absorption at 1167 and  $1358 \text{ km s}^{-1}$ . These absorbers both have the correct velocity *sign*, but we would expect a smaller velocity for co-rotation (approximately  $\Delta v \sim \pm 40 \text{ km s}^{-1}$  projected). This difference could be explained by invoking either a warped extended disk, or perhaps inflowing gas.

1H0419-577 is located to the south at 303 kpc and just east of the receding side of the major axis at an azimuth angle of  $10^\circ$ . We detect Ly $\alpha$  at 1071, 1123, 1188, 1264, and  $2020 \text{ km s}^{-1}$ , all of which are the wrong sign for co-rotation or distant in velocity. This sightline

is actually closer to a small group of galaxies including NGC1549, NGC1546 and NGC1536, all with systemic velocities near  $1200 \text{ km s}^{-1}$ . We expect the lines at 1071, 1123, 1188,  $1264 \text{ km s}^{-1}$  to be associated with this group rather than with NGC1566.

#### 4.6. NGC3513

NGC3513 a mostly face-on SB(rs)c galaxy with heliocentric velocity  $V_{\text{hel}} = 1204 \pm 12 \text{ km s}^{-1}$ . It has a companion galaxy in NGC3511 at an impact parameter of 44 kpc at  $v_{\text{hel}} = 1109 \text{ km s}^{-1}$ . We detect Ly $\alpha$  at  $1182 \text{ km s}^{-1}$  toward background QSO H1101-232, which is located directly south at 60 kpc and azimuth angle of  $67^\circ$  on the receding side. NGC3513 appears to be rotating slowly, with a maximal inclination-corrected rotation velocity of  $22 \pm 24 \text{ km s}^{-1}$ . The  $\Delta v = -22 \text{ km s}^{-1}$  for this absorber matches well with the magnitude of this rotation, but is opposite in sign for co-rotation. Given that NGC3511 is so close, this absorber's velocity is probably subject to a complex velocity field influenced by both NGC3511 and NGC3513.

#### 4.7. NGC3633

NGC3633 is an isolated, edge-on SAa type galaxy at a velocity of  $2587 \pm 7 \text{ km s}^{-1}$ . Several locations along the disk of NGC3633 show two velocities for emission. We have combined these into a single velocity measurement via a weighted average. There are three nearby sightlines: SDSSJ112005.00+041323.0 is straight north at 468 kpc and  $78^\circ$  azimuth, RX\_J1121.2+0326 is to the southeast at 184 kpc and  $58^\circ$  azimuth, and SDSSJ112224.10+031802.0 at 413 kpc and  $50^\circ$  azimuth. Toward RX\_J1121.2+0326 we detect a Ly $\alpha$  absorber at  $2605 \text{ km s}^{-1}$  on the approaching side, which is essentially systemic velocity for NGC3633. The spectrum of SDSSJ112224.10+031802.0 shows absorbers at 2285 and  $2578 \text{ km s}^{-1}$ , both of which are of the correct sign for co-rotation. We do not detect any Ly $\alpha$  towards the third



sightline, SDSSJ112224.10+031802.0.

#### 4.8. NGC4536

NGC4536 is a SAB(rs)bc type galaxy located in a complex environment with many other nearby galaxies. The data on the receding side of NGC4536 is quite messy, and may include contamination from background sources. Hence, our measured systemic velocity of  $1867 \pm 33 \text{ km s}^{-1}$ , and thus rotation velocity of  $139 \pm 37 \text{ km s}^{-1}$ , have relatively high uncertainty. Other published redshift values available from NED and rotation velocities from the HyperLEDA database are broadly consistent with our values, albeit biased slightly lower and higher in velocity, respectively.

There are 2 sightlines to the southwest of NGC4536, both on the receding side of the galaxy. HE1228+0131 at 338 kpc and  $86^\circ$  azimuth has 5 Ly $\alpha$  lines: 1495, 1571, 1686, 1721, and  $1854 \text{ km s}^{-1}$ . None of these are of the correct orientation for co-rotation, and all are more likely to be associated with other nearby galaxies, such as NGC4517A, which is slightly closer to these absorbers in impact parameter and velocity than is NGC4536. The second nearby sightline is toward 3C273 at 344 kpc and  $46^\circ$  azimuth angle, and shows 3 Ly $\alpha$  lines at velocities of 1580, 2156,  $2267 \text{ km s}^{-1}$ . Two of these are correctly oriented for co-rotation, but are too high in velocity to make this scenario probable. Overall, given the number of nearby galaxies and their locations, we would expect these absorbers to trace the overall velocity field instead of the halo rotation of any particular galaxy.

#### 4.9. NGC4939

NGC4939 is a large, fast rotating ( $V_{rot} = 275 \pm 49 \text{ km s}^{-1}$ ) SA(s)bc type galaxy at systemic velocity  $V_{hel} = 3093 \pm 33 \text{ km s}^{-1}$ . We detect a single Ly $\alpha$  absorber at  $3448 \text{ km s}^{-1}$  towards PG1302-102 at 254 kpc and  $61^\circ$  azimuth angle towards the southeast. This absorber is located on the approaching side of this galaxy, so we can easily rule out co-rotation in this case. NGC4939 does not have any close neighbors, so represents strong case against co-rotation for gas near or past  $1 R_{vir}$ .

#### 4.10. NGC5364

NGC5364 is a SA(rs)bc pec type galaxy at a measured systemic velocity of  $1238 \pm 17 \text{ km s}^{-1}$ . It is located in a group environment with 5 other large, nearby galaxies. The sightline toward SDSSJ135726.27+043541.4 at 165 kpc and  $84^\circ$  azimuth angle contains Ly $\alpha$  absorbers at 1124 and  $1296 \text{ km s}^{-1}$  on the receding side. However, because of the orientation of NGC5364 on the sky with respect to this sightline, these absorbers lie extremely close to the inflection point where projected rotation velocities flip to approaching instead of receding. For example, shifting the location of SDSSJ135726.27+043541.4 east by a tenth of a degree ( $\sim 20 \text{ kpc}$ ) is sufficient to put these absorbers on the approaching side of NGC5364. Hence, both of these absorbers could be co-rotating with NGC5364 given very reasonable assumptions on

the shape of an extended disk. Nonetheless, the fact that this system lives in galaxy group environment likely dominates the surrounding velocity field.

#### 4.11. NGC5786

NGC5786 is a large, strongly-barred spiral galaxy at  $V_{sys} = 2975 \pm 22$ . The sole nearby sightline lies along the major axis on the receding side of NGC5786 at 453 kpc toward QSO1500-4140. Unfortunately for the purpose of this exercise, there are two neighboring galaxies, both of which are closer than this. ESO327-G038 and ESO327-G039 are both located directly south at 62 kpc and 296 kpc, respectively. Toward QSO1500-4140 we detect Ly $\alpha$  absorption at  $3138 \text{ km s}^{-1}$ , corresponding to a velocity difference  $\Delta v = 163 \text{ km s}^{-1}$ . Although this velocity aligns nicely with expected co-rotation velocities, the nearby neighboring galaxies and large distance to the absorption ( $\sim 2.5 R_{vir}$ ) make it difficult to believe this as evidence of an extended disk.

#### 4.12. UGC09760

UGC09760 is an edge-on, slow-rotating Sd galaxy with a single sightline toward SDSSJ151237.15+012846.0 located 123 kpc away along the minor axis. Our measured systemic velocity,  $V_{sys} = 2094 \pm 16$ , deviates slightly from other published redshifts, such as the The Updated Zwicky Catalog value of  $V_{sys} = 2023 \pm 2$  (Falco et al. 1999). We detect Ly $\alpha$  absorption at  $2051 \text{ km s}^{-1}$  ( $\Delta v = -43 \text{ km s}^{-1}$ ). This velocity matches well with the rotation velocity of UGC09760 ( $V_{rot} = 46 \pm 16 \text{ km s}^{-1}$ ), but unfortunately this sightline lies almost exactly at an azimuth of  $90^\circ$ . Hence, the motion of this gas could easily be either co-rotating or counter-rotating depending on a minute change in the position angle assigned to UGC09760. This is especially true if we assume our measured  $V_{sys}$  is erroneously high, and indeed closer to the values obtained by other observations.

It is worth noting that there are several small satellite galaxies nearby, including SDSSJ151208.16+013508.5, SDSSJ151121.63+013637.6, SDSSJ151241.38+013723.7 and UGC09746 (impact parameters of 53, 88, 82, 230 kpc respectively). All of these galaxies lie slightly blueward of UGC09760, and thus *farther* away in velocity from the Ly $\alpha$  absorber at  $2051 \text{ km s}^{-1}$ .

### 5. ANCILLARY DATA

To increase our sample size we have also searched the literature for galaxies with published rotation curves and orientations. Unfortunately, while the rotation velocity is available for thousands of galaxies, only a handful also include the *orientation* of the rotation on the sky. Of these, we were able to find 18 additional galaxies which have a systemic velocity greater than  $\sim 500 \text{ km s}^{-1}$ , and are near to a COS or STIS sightline with available data.

#### 5.1. NGC3198

NGC3198 is a well studied SB(rs)c type galaxy which is included the detailed THINGS rotation curve study

of [de Blok et al. \(2008\)](#). We extracted the raw rotation curve derived by [de Blok et al. \(2008\)](#) using the plot digitization software WebPlotDigitizer<sup>2</sup>. NGC3198 has a systemic velocity of  $660 \text{ km s}^{-1}$ , and is located 370 kpc away from a sightline toward RX\_1017.5+4702 at an azimuth angle of  $55^\circ$  on the approaching side of NGC3198 (northeast). NGC3198 has an even and flat rotation curve, with an average velocity of  $v_{rot} = 152 \text{ km s}^{-1}$  and an expected velocity range of  $[-82, -23]$  based on our projected NFW profile fit. We detect Ly $\alpha$  absorption in the spectrum of RX\_1017.5+4702 at  $629 \text{ km s}^{-1}$  ( $\Delta v = -31 \text{ km s}^{-1}$ ). Hence, the velocity of this absorber can nicely be described by a co-rotating disk.

SDSSJ101622.60+470643.0 is also located in the same direction but at a more distant 401 kpc away (**NOT IDENTIFIED**).

The small dwarf galaxy SDSSJ101848.77+452137.0 is located 65 kpc away toward the southwest.

### 5.2. NGC3351

[Mazzalay et al. \(2014\)](#)

778kms - no rot curve yet - close to a big group  
 IRAS10378+1109 - no data (clobbered by LLS)  
 3C245.0 - low res only  
 SDSSJ104335.90+115129.0 at 31kpc, 13 az (Lya at 717, 882, 1030)  
 SDSSJ104816.30+120735.0 at 198kpc, 85 az (G130M but not in reduce)  
 SDSSJ104709.80+130454.0 at 277kpc, 47 az (G130M but not in reduce)  
 SDSSJ104843.50+130605.0 at 317kpc, 57 az (G130M but not in reduce)  
 SDSSJ105125.80+124746.0 at 371, 76 az (proprietary until 2019)  
 SDSSJ105220.60+101751.0 at 435kpc, 39 az (not ID'd, possible line)  
 SDSSJ104341.53+085558.2 at 484kpc, 18 az (G130M but not in reduce)

### 5.3. NGC5907

- 667kms - Sanders 1996, Allaert (2015A&A...582A..18A) also

NW is receding side ([Allaert et al. 2015](#)).  
 Rotation curve data from [Yim et al. \(2014\)](#)

SDSSJ152053.59+571122.1 at 286kpc, (possible line, messy spectrum)  
 SBS1503+570 at 413kpc, 47 az (Lya at 708kms)

### 5.4. NGC4565

NGC4565 is an edge on ( $i = 75^\circ$  at a heliocentric velocity of  $1230 \text{ km s}^{-1}$ , for which we have taken the

rotation curve and orientation from [Sofue \(1996\)](#).  
 RX\_J1236.0+2641 at 147kpc (Lya at 794, 1009, 1166 kms)

### 5.5. UGC06446

$V_{sys} = 645 \text{ km s}^{-1}$ . ([Swaters et al. 2009](#); [Verheijen & Sancisi 2001](#))  
 MCG9-19-073 at 179kpc - low res only  
 SDSSJ112448.30+531818.0 at 143kpc, 22 az (Lya at 664kms)  
 RBS971 at 226kpc, 88 az (clobbered by huge H2 system)  
 RX\_J1117.6+5301 at 417kpc, 52 az (Lya at 685kms)

### 5.6. UGC06399

$V_{sys} = 791 \text{ km s}^{-1}$ . [Swaters et al. \(2009\)](#)  
 SBS1116+523 at 471kpc, 13.4 az (Lya at 731kms)  
 MCG9-19-078 at 301kpc (G160M only)

### 5.7. NGC3726

$V_{sys} = 866 \text{ km s}^{-1}$ . S side is receding. [Verheijen & Sancisi \(2001\)](#)

Inclination: 52  
 Adjusted Inc: 54  
 Morphology: SAB(r)c  
 $L_* = 1.5$

CSO1208 at 369kpc, 87 az (Lya at 731, 874kms)  
 PGC139665 at 440, 86 az (G130M but not in reduce)  
 close to CSO1208

Both sightlines closer to some other little galaxies.  
 NGC3877 nearby, has rot curve

### 5.8. NGC3067

The galaxy-QSO pair NGC3067-3C232 is a particularly well studied system. They are separated by only 11 kpc ( $74^\circ$  azimuth angle) and a LLS of  $N_{HI} = 110^{20} \text{ cm}^{-2}$  is detected toward 3C232 at  $1421 \text{ km s}^{-1}$  ( $V_{sys} = 1476 \text{ km s}^{-1}$ ), which has been postulated as a high velocity cloud (HVC) orbiting NGC3067. We obtained the rotation curve for NGC3067 from [Danziger & Chromey \(1972\)](#) and the orientation from [Carilli et al. \(1989\)](#) (see also [Keeney et al. \(2005\)](#)).

Inclination: 68  
 Adjusted Inc: 71  
 Morphology: SAB(s)ab  
 $L_* = 0.5$

SDSSJ095914.80+320357.0 at 128 kpc, 43 az (no ID'd, but probable line around 1500kms)  
 RX\_J1002.9+3240 at 359 kpc, 33 az (not in reduce yet)

<sup>2</sup> WebPlotDigitizer; <http://arohatgi.info/WebPlotDigitizer>

We have also included the 5 galaxy-QSO systems analyzed by Côté et al. (2005). We briefly summarize each of these systems here, and refer the reader to Côté et al. (2005) for a more complete discussion. **ALL? OF THESE GALAXIES WE PROJECT TO BE AT GREATER IMPACT PARAMETER THAN COTE DID. MOSTLY BASED ON BETTER RID DISTANCES THAN USED BY COTE**

#### 5.9. NGC6140

NGC6140 is a small SB(s)cd pec type galaxy located at  $V_{sys} = 910 \text{ km s}^{-1}$  and 113 kpc from the sightline toward QSO MRK876. The approaching side is oriented toward the east, with MRK876 toward the northwest at an azimuth of  $55^\circ$  (although this is somewhat uncertain; the position angle for NGC6140 could be closer to  $90^\circ$  than our adopted value of  $60^\circ$  due to it being mostly face on, faint, and strongly barred).

Inclination: 44  
Adjusted Inc: 45  
Morphology: SB(s)cd  
 $L_* = 0.2$

#### 5.10. NGC4529

As an inclined, isolated galaxy with a QSO sightline located 159kpc and only  $23^\circ$  off the major axis, NGC4529 represents an ideal test environment for this study. This sightline towards MRK771 contains a Ly $\alpha$  absorber at  $2553 \text{ km s}^{-1}$ . With  $V_{sys} = 2536 \text{ km s}^{-1}$  and MRK771 located on the approaching side of NGC4529 (SW side), this is a clearcut case of counterrotating *Hi*. As Côté et al. (2005) conclude, “there is simply no physical way to produce such a velocity with an extending co-rotating disk.”

Inclination: 69  
Adjusted Inc: 72  
Morphology: Scd  
 $L_* = 1.2$

#### 5.11. UGC04238

Rotation curve taken from Côté et al. (2005).

Inclination: 77  
Adjusted Inc: 75  
Morphology: SBd  
 $L_* = 0.58$

PG0804+761 at 148kpc

The following are from Rhee & van Albada (1996):

#### 5.12. NGC2770

$V_{sys} = 1947 \text{ km s}^{-1}$ . Nearby to small dwarfs MCG+06-20-036NED02 and GALEX-ASCJ090946.88+330840.4 (both 25 kpc, on opposite

sides of NGC2770). Rhee & van Albada (1996)

Inclination: 75  
Adjusted Inc: 80  
Morphology: SA(s)c  
 $L_* = 1.8$

FBQSJ0908+3246 at 204 kpc, 59 az (Lya at 1915, 1982)  
TON1009 at 267 kpc - used to be identified, but not anymore?  
TON1015 at 218 kpc, 61 az (Lya at 1833, 1985)  
SDSSJ091052.80+333008.0 at 239 kpc, 66 az (Lya at 1824, 1975)  
SDSSJ091127.30+325337.0 at 234 kpc, 30 az (Lya at 2063)

#### 5.13. NGC3432

$V_{sys} = 616 \text{ km s}^{-1}$ . Interacting with the nearby dwarf galaxy UGC05983 located 11 kpc away and at  $V_{sys} = 765 \text{ km s}^{-1}$ . Rhee & van Albada (1996).

Inclination: 78  
Adjusted Inc: 90  
Morphology: SB(s)m  
 $L_* = 0.42$

CSO295 at 20 kpc, 82 az  
RX\_J1054.2+3511 at 290 kpc, 57 az  
MS1047.3+3518 at 326 kpc, 26 az

#### 5.14. NGC3666

$V_{sys} = 1060 \text{ km s}^{-1}$ . Mostly isolated, with only a few dwarfs  $\sim 400$  kpc away. Rhee & van Albada (1996)

Inclination: 73  
Adjusted Inc: 77  
Morphology: SA(rs)c  
 $L_* = 0.61$

SDSSJ112439.50+113117.0 at 58 kpc - Borthakur target (not in reduce yet)  
SDSSJ112632.90+120437.0 at 279 kpc - Borthakur target (not in reduce yet)  
SDSSJ112756.70+115427.0 at 320 kpc - (not in reduce yet)  
SDSSJ111916.20+110107.0 at 406 kpc - G230L only  
4C12.40 at 451 kpc - G190H, G270H, G230L only

#### 5.15. NGC5951

$V_{sys} = 1780 \text{ km s}^{-1}$ . A couple of nearby galaxies (NGC5954, NGC5953), but the sightline is closer and on the opposite side. Rhee & van Albada (1996)

Inclination: 78  
Adjusted Inc: 86

Morphology: SBc  
 $L_* = 1.4$

2E1530+1511 at 55 kpc, 85 az - (Lya at 1795, 1953)

#### 5.16. NGC7817

$V_{sys} = 2309 \text{ km s}^{-1}$ . Sightline toward MRK335 is equidistant but opposite NGC7798. Rhee & van Albada (1996)

Inclination: 75  
 Adjusted Inc: 80  
 Morphology: SABc  
 $L_* = 0.79$

MRK335 at 343 kpc, 90 az (Lya at 1954, 2274)

#### 5.17. UGC08146

$V_{sys} = 670 \text{ km s}^{-1}$ . Small but isolated. Rhee & van Albada (1996). This galaxy also is included in the Côté et al. (2005) sample.

Inclination: 78  
 Adjusted Inc: 90  
 Morphology: Scd  
 $L_* = 0.31$

PG1259+593 at 114 kpc, 50 az (Lya at 646, 683)  
 SBS1304+594 at 235 kpc, 15 az (no lines, low SN)

## 6. DISCUSSION

## 7. SUMMARY

This research has made use of the NASA/IPAC Extragalactic Database (NED) which is operated by the Jet Propulsion Laboratory, California Institute of Technology, under contract with the National Aeronautics and Space Administration. Based on observations with the NASA/ESA *Hubble Space Telescope*, obtained at the Space Telescope Science Institute (STScI), which is operated by the Association of Universities for Research in Astronomy, Inc., under NASA contract NAS 5-26555. **SALT ACKNOWLEDGEMENT.** Spectra were retrieved from the Barbara A. Mikulski Archive for Space Telescopes (MAST) at STScI. Over the course of this study, D.M.F. and B.P.W. were supported by grant AST-1108913, awarded by the US National Science Foundation, and by NASA grants *HST*-AR-12842.01-A, *HST*-AR-13893.01-A, and *HST*-GO-14240 (STScI).

*Facility:* HST (COS)

## APPENDIX

### A. ROTATION CURVES

Here we present rotation curves with finder charts indicating the slit position for each galaxy observed with SALT.

## REFERENCES

- Allaert, F., Gentile, G., Baes, M., et al. 2015, *A&A*, 582, A18  
 Bowen, D. V., Chelouche, D., Jenkins, E. B., et al. 2016, *ApJ*, 826, 50  
 Carilli, C. L., van Gorkom, J. H., & Stocke, J. T. 1989, *Nature*, 338, 134  
 Côté, S., Wyse, R. F. G., Carignan, C., Freeman, K. C., & Broadhurst, T. 2005, *ApJ*, 618, 178  
 Danziger, I. J., & Chromey, F. R. 1972, *Astrophys. Lett.*, 10, 99  
 de Blok, W. J. G., Walter, F., Brinks, E., et al. 2008, *AJ*, 136, 2648  
 Falco, E. E., Kurtz, M. J., Geller, M. J., et al. 1999, *PASP*, 111, 438  
 French, D. M., & Wakker, B. P. 2017, *ApJ*, 837, 138  
 Green, J. C., Froning, C. S., Osterman, S., et al. 2012, *ApJ*, 744, 60  
 Keeney, B. A., Momjian, E., Stocke, J. T., Carilli, C. L., & Tumlinson, J. 2005, *ApJ*, 622, 267  
 Mazzalay, X., Maciejewski, W., Erwin, P., et al. 2014, *MNRAS*, 438, 2036  
 Navarro, J. F., Frenk, C. S., & White, S. D. M. 1996, *ApJ*, 462, 563  
 —. 1997, *ApJ*, 490, 493  
 Rhee, M.-H., & van Albada, T. S. 1996, *A&AS*, 115, 407  
 Sofue, Y. 1996, *ApJ*, 458, 120  
 Stewart, K. R., Brooks, A. M., Bullock, J. S., et al. 2013, *ApJ*, 769, 74  
 Stewart, K. R., Kaufmann, T., Bullock, J. S., et al. 2011, *ApJ*, 738, 39  
 Swaters, R. A., Sancisi, R., van Albada, T. S., & van der Hulst, J. M. 2009, *A&A*, 493, 871  
 Verheijen, M. A. W., & Sancisi, R. 2001, *A&A*, 370, 765  
 Wakker, B. P., Hernandez, A. K., French, D. M., et al. 2015, *ApJ*, 814, 40  
 Wakker, B. P., & Savage, B. D. 2009, *ApJS*, 182, 378  
 Yim, K., Wong, T., Xue, R., et al. 2014, *AJ*, 148, 127



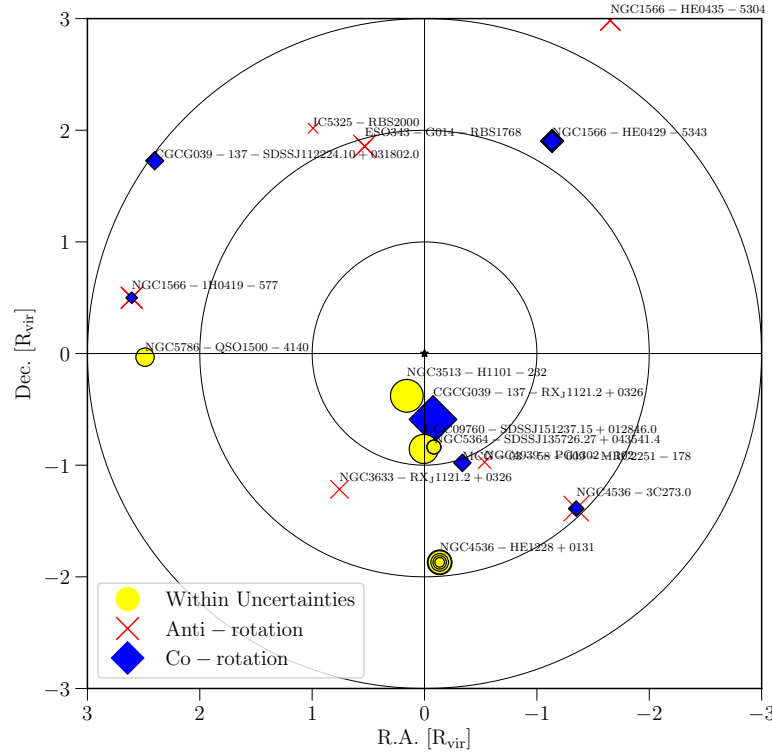


**Figure 1.** A map of the locations of each absorber normalized with respect to the galaxy virial radius. Concentric rings indicate distances of 1, 2 and 3  $R_{vir}$ . All galaxies are rotated to  $PA = 90$ , such that their major axis' are horizontal. The color and style of each point indicates the line-of-sight velocity compared to that of the rotation of the nearby galaxy. Blue diamonds indicate co-rotation, red X's indicate anti-rotation, and yellow circles indicate cases where either is possible due to a combination of orientation and velocity uncertainties. The size of each point is scaled to reflect the EW of the absorber.

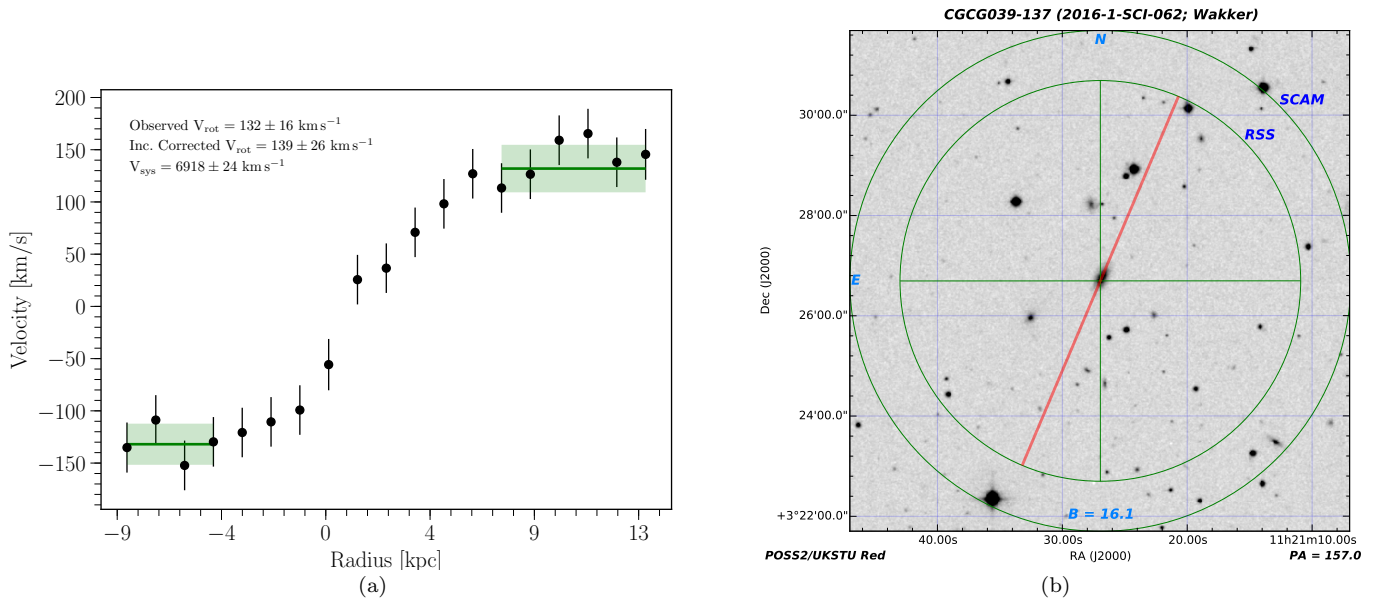


**Figure A1.** a) Rotation curve of CGCG039-137. The solid green line indicates the weighted mean velocity over the corresponding x-axis region, and the shaded green indicates the  $1\sigma$  error in the mean. b) SALT finder chart for CGCG039-137 showing the position of the slit in red.

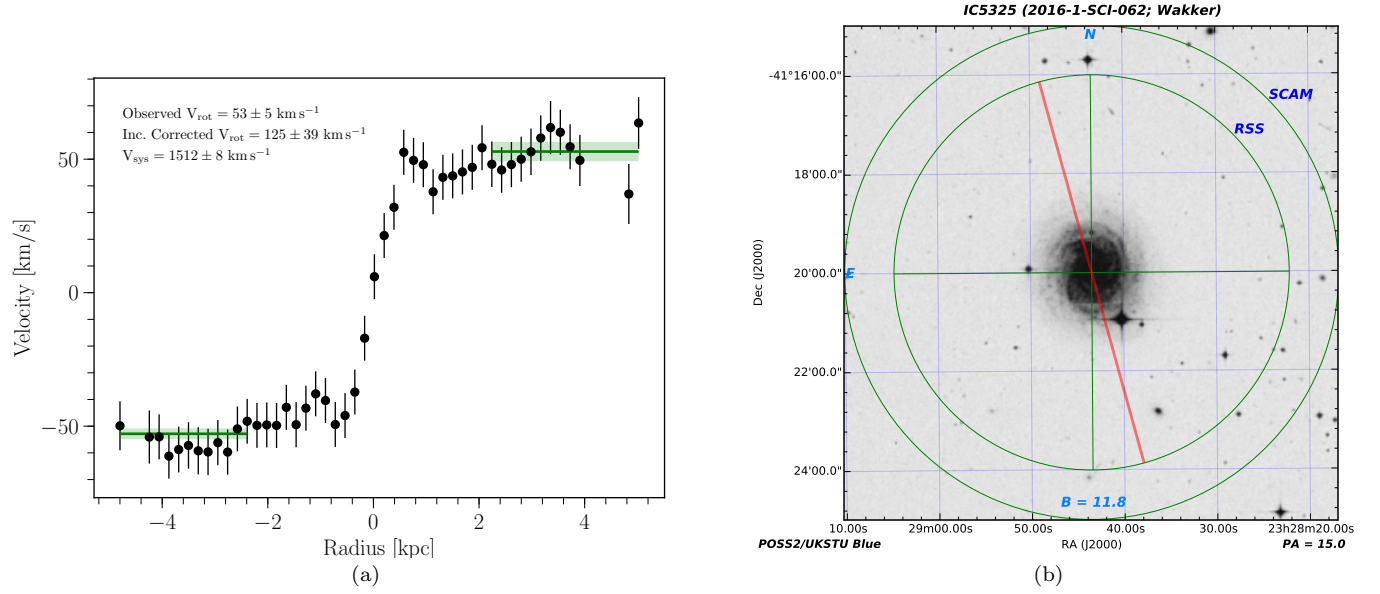


**Figure A2.** a) Rotation curve of IC5325. The solid green line indicates the weighted mean velocity over the corresponding x-axis region, and the shaded green indicates the  $1\sigma$  error in the mean. b) SALT finder chart for IC5325 showing the position of the slit in red.

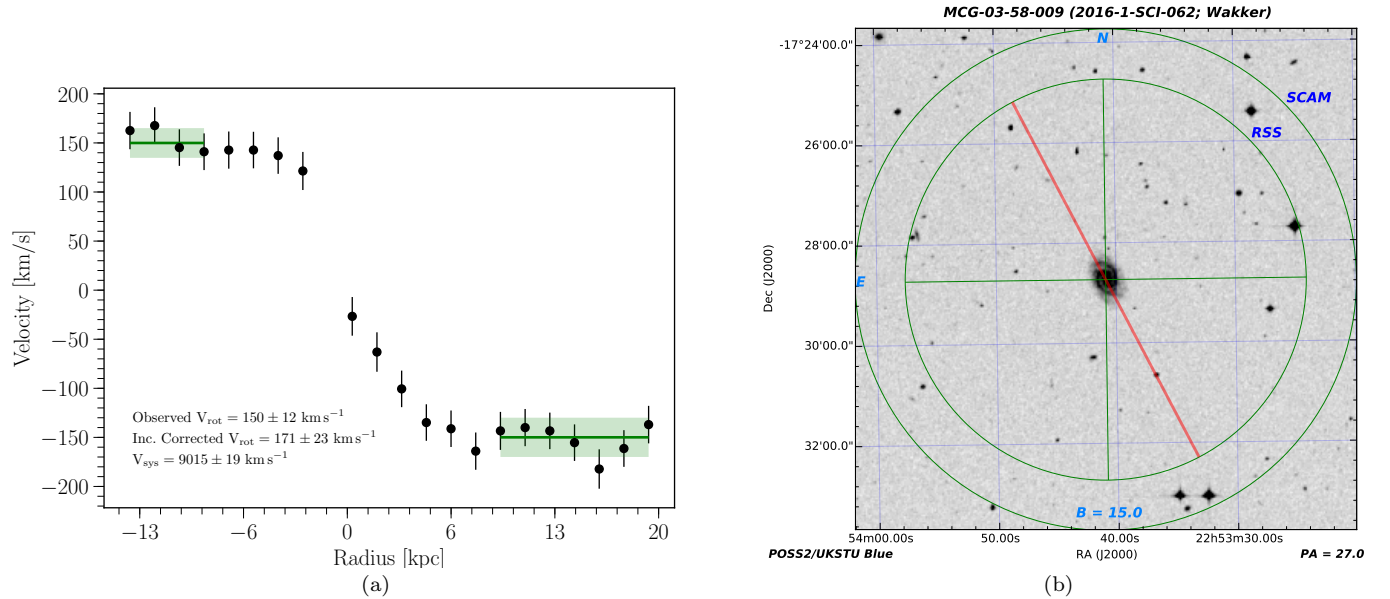


**Figure A3.** a) Rotation curve of MCG-03-58-009. The solid green line indicates the weighted mean velocity over the corresponding x-axis region, and the shaded green indicates the  $1\sigma$  error in the mean. b) SALT finder chart for MCG-03-58-009 showing the position of the slit in red.

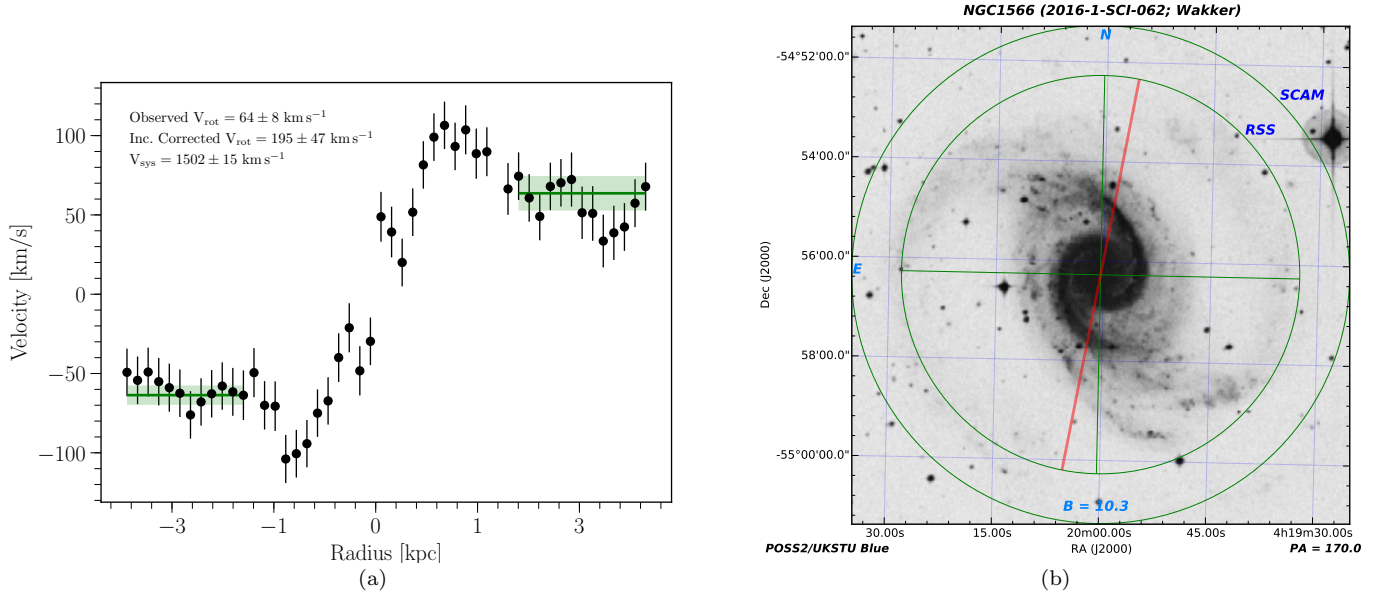


**Figure A4.** a) Rotation curve of NGC1566. The solid green line indicates the weighted mean velocity over the corresponding x-axis region, and the shaded green indicates the  $1\sigma$  error in the mean. b) SALT finder chart for NGC1566 showing the position of the slit in red.

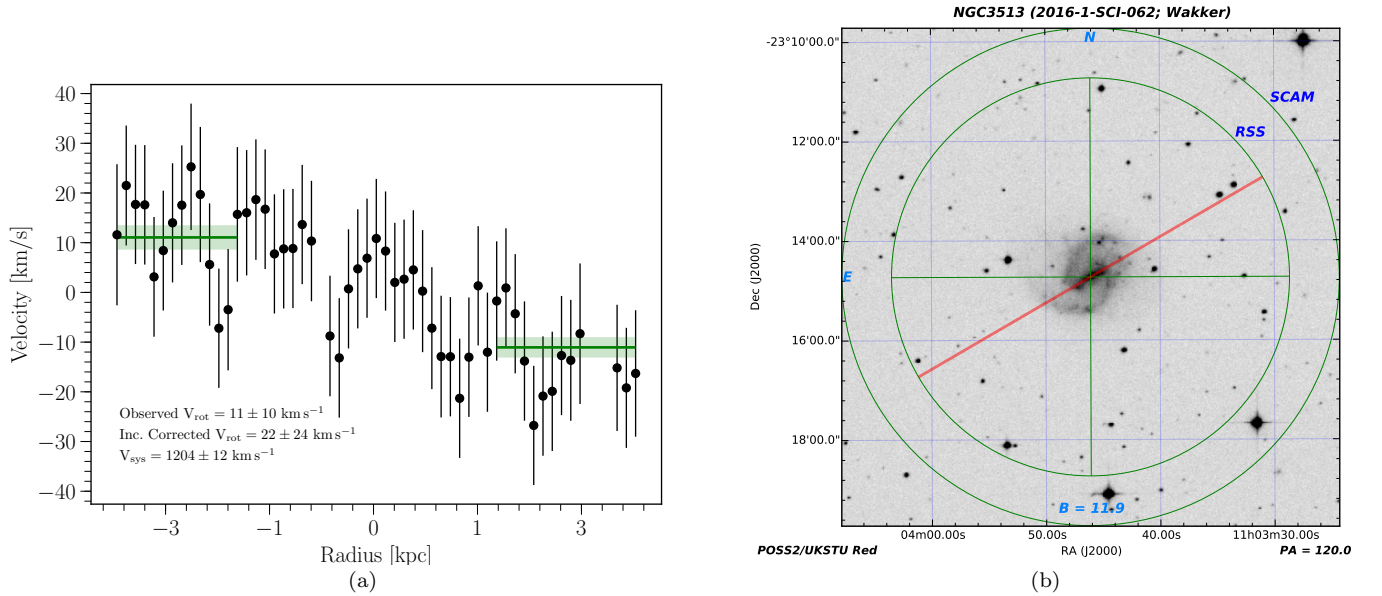


**Figure A5.** a) Rotation curve of NGC3513. The solid green line indicates the weighted mean velocity over the corresponding x-axis region, and the shaded green indicates the  $1\sigma$  error in the mean. b) SALT finder chart for NGC3513 showing the position of the slit in red.

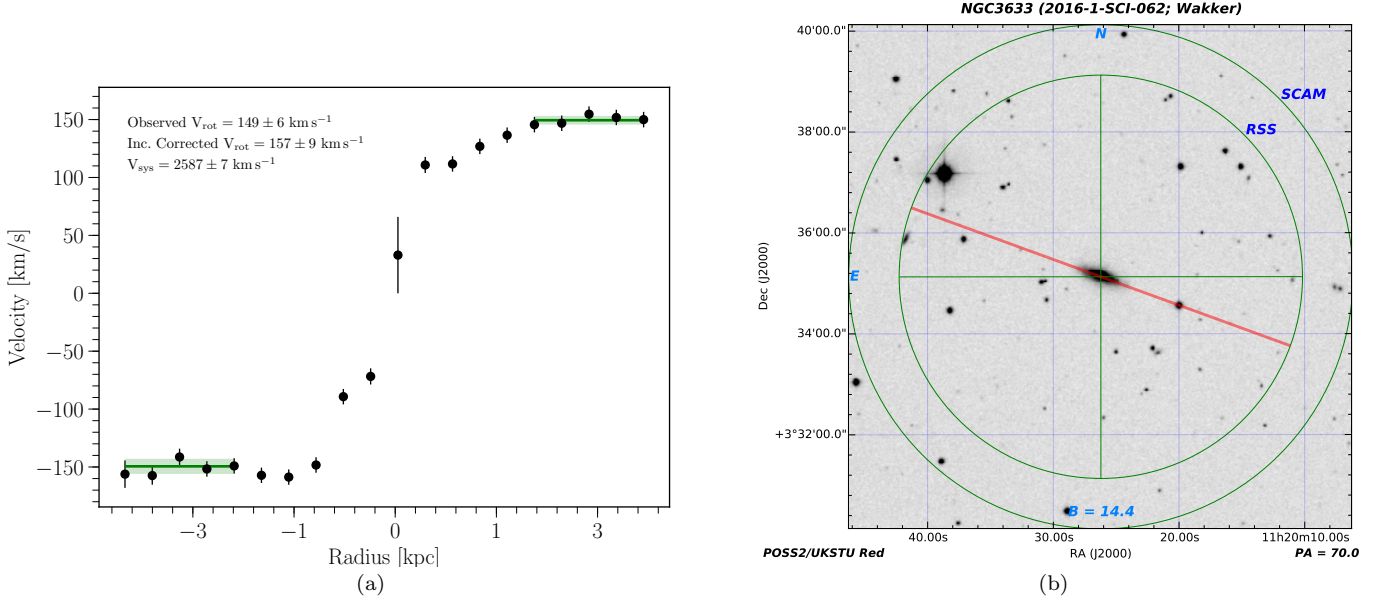


**Figure A6.** a) Rotation curve of NGC4536. The solid green line indicates the weighted mean velocity over the corresponding x-axis region, and the shaded green indicates the  $1\sigma$  error in the mean. b) SALT finder chart for NGC3633 showing the position of the slit in red.

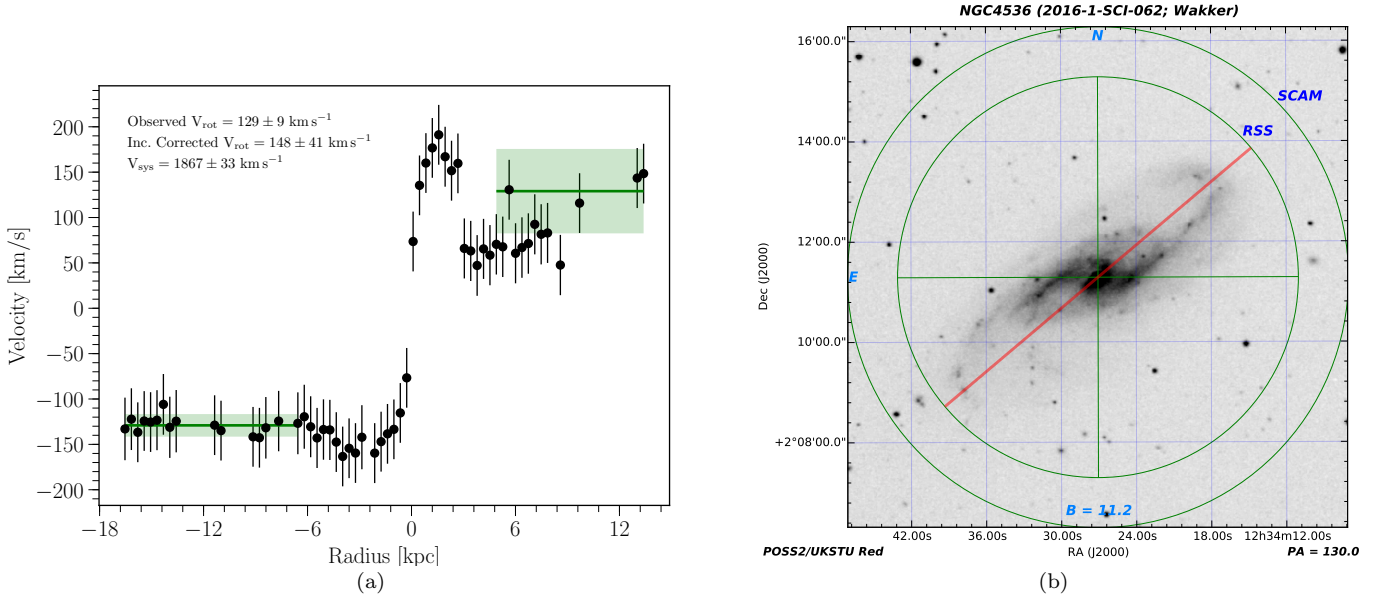


**Figure A7.** a) Rotation curve of NGC4536. The solid green line indicates the weighted mean velocity over the corresponding x-axis region, and the shaded green indicates the  $1\sigma$  error in the mean. b) SALT finder chart for NGC4536 showing the position of the slit in red.

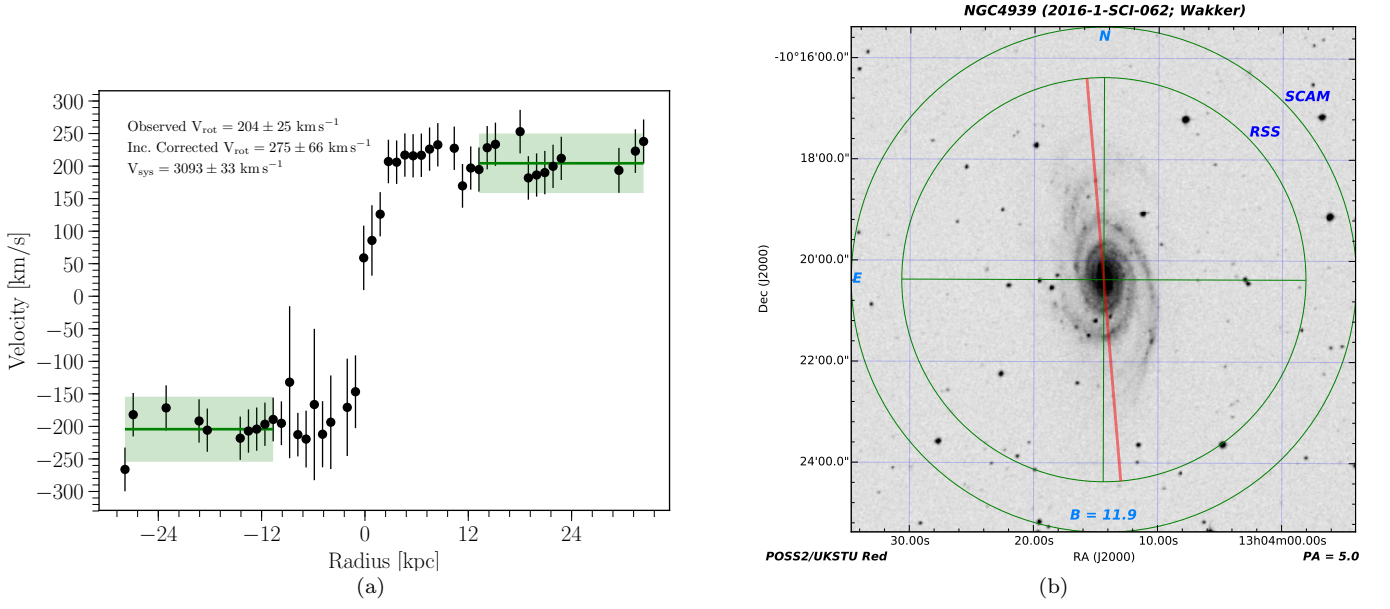


**Figure A8.** a) Rotation curve of NGC4939. The solid green line indicates the weighted mean velocity over the corresponding x-axis region, and the shaded green indicates the  $1\sigma$  error in the mean. b) SALT finder chart for NGC4939 showing the position of the slit in red.

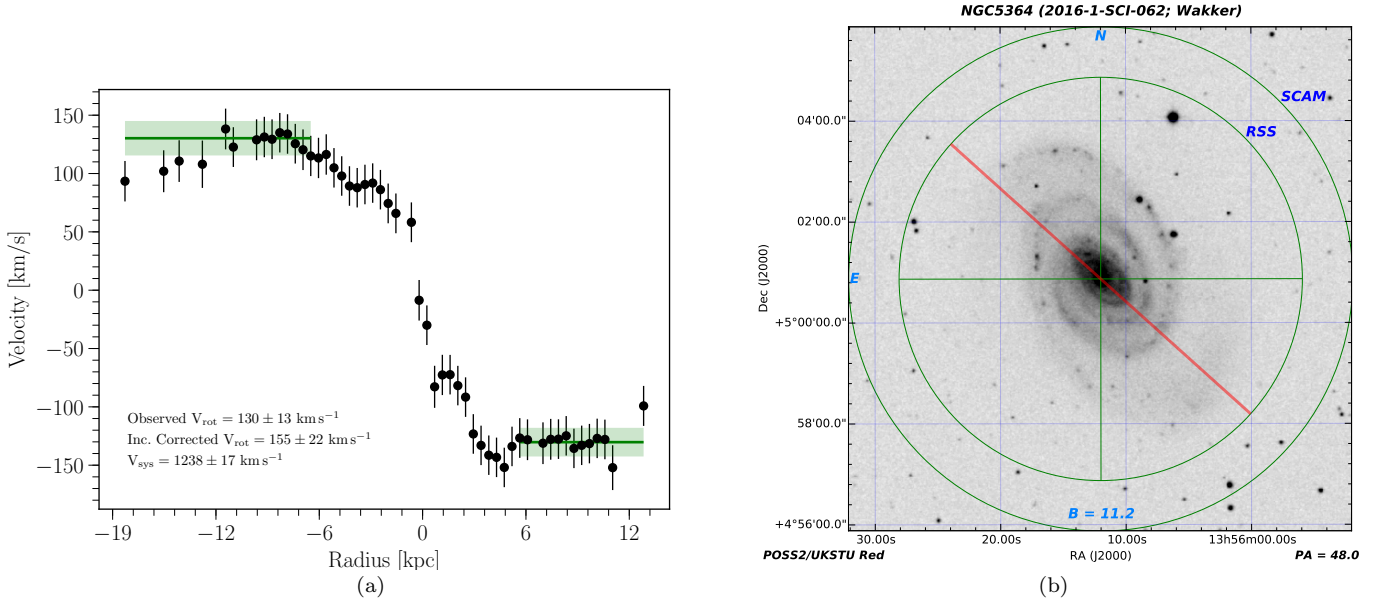


**Figure A9.** a) Rotation curve of NGC5364. The solid green line indicates the weighted mean velocity over the corresponding x-axis region, and the shaded green indicates the  $1\sigma$  error in the mean. b) SALT finder chart for NGC5364 showing the position of the slit in red.



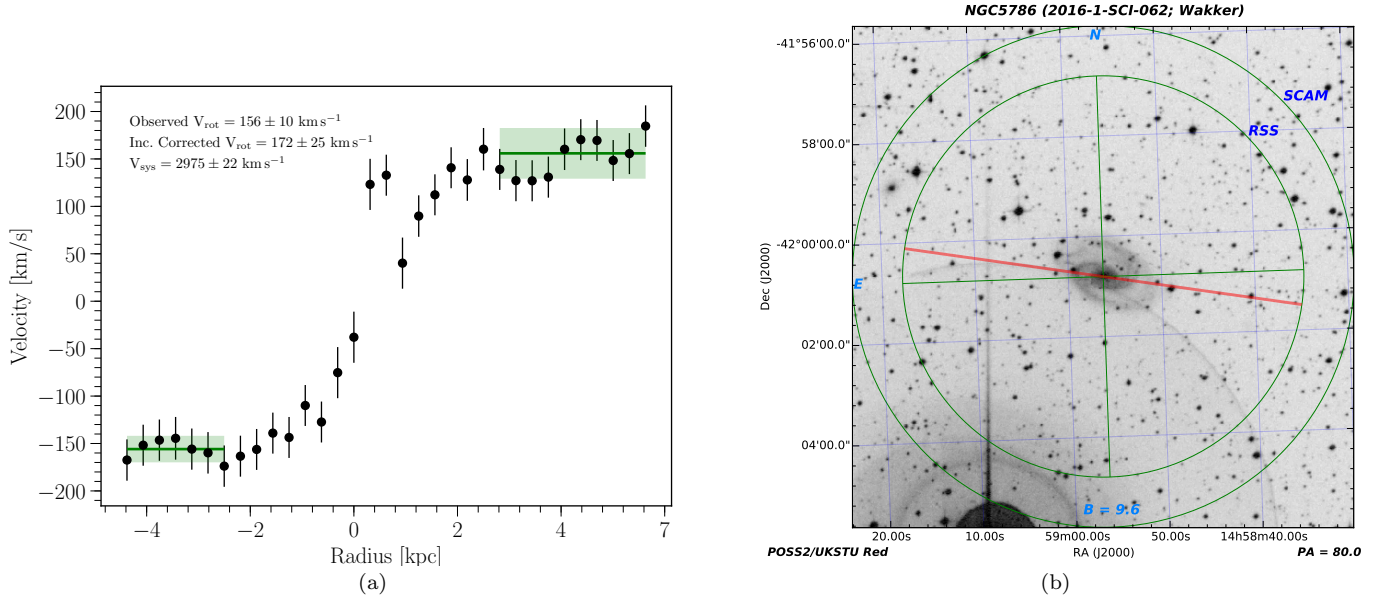


**Figure A10.** a) Rotation curve of NGC5786. The solid green line indicates the weighted mean velocity over the corresponding x-axis region, and the shaded green indicates the  $1\sigma$  error in the mean. b) SALT finder chart for NGC5786 showing the position of the slit in red.

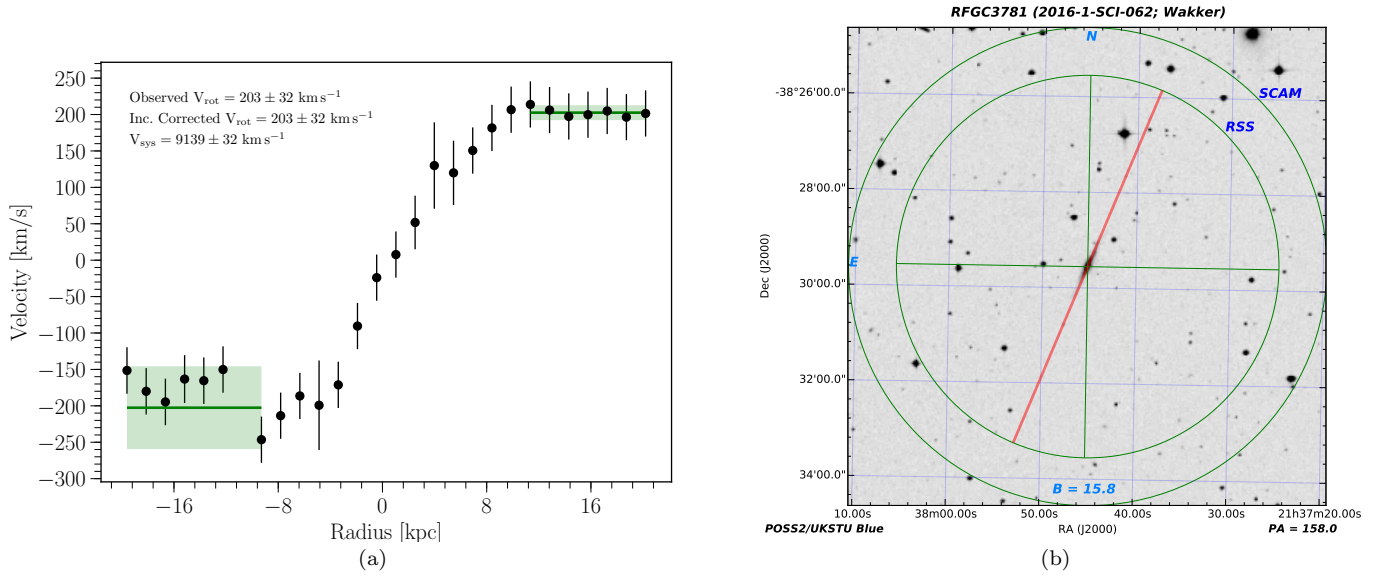


**Figure A11.** a) Rotation curve of NGC5364. The solid green line indicates the weighted mean velocity over the corresponding x-axis region, and the shaded green indicates the  $1\sigma$  error in the mean. b) SALT finder chart for NGC5364 showing the position of the slit in red.